Optics of a two-stage collimation system

J.B. Jeanneret
CERN, CH-1211 Geneva, Switzerland

We derive the exact specification that a two-stage betatronic collimation insertion must satisfy to cut the halo of a proton beam down to its ultimate limit which is the aperture of the secondary collimators. Our result is a set of correlated phase advances between primary and secondary collimators. We then determine the number of jaws needed to reach a given level of performance. We also specify the optic of a momentum collimation insertion.

I. INTRODUCTION

In superconducting proton colliders of both high energy and high beam current the control of beam losses is mandatory. Local power deposition associated to beam losses can be larger than the quench level of superconducting magnets by several orders of magnitude [1]. In addition the large size of the rings at high energy imply to keep the transverse size of the magnets small for obvious cost reasons. Therefore the geometrical aperture delimited by the vacuum chamber must be kept to its bare minimum. Beam losses are mostly related to beam dynamics. Not far above the dynamic aperture the transverse motion of the particles becomes chaotic and can form a halo diffusing towards the geometrical aperture. The transverse extension of the halo is limited by absorbing these protons in collimators which are made of metallic blocks, which are called jaws below. The jaws inserted close to the beam are called primary collimators and define the primary aperture which is normally chosen to be larger or equal to the dynamic aperture in order not to intercept stable particles. At all energies the absorbtion of protons in primary jaws is substantially distant from unity [1]. Protons which are not absorbed can be scattered elastically off the jaw thus forming a secondary halo which can also induce quenches. Secondary jaws are therefore necessary to limit the extension of the secondary halo to a value smaller than the geometrical aperture or, otherwise said, to allow for the choice of a small but safe geometrical aperture.

The geometrical size of the secondary halo, normalised to the aperture of the collimators, depends on the number of jaws, on their relative locations and on the optic of the insertion where they are installed.

An exact treatment of a two-stage collimation system considered as an optical device, i.e disregarding true scattering in collimator jaws, exist for the one-dimensional case (1D) and in the special two-dimensional case (2D) of an optic with equal phase advance in the two transverse dimensions [2]. The problem of a 2D-system with an arbitrary optic was solved with numerical methods in conjunction with the approximate concept of phase modulation with some success [2] [3], but without cutting the amplitude of the secondary halo down to the ultimate limit of the aperture of the secondary collimators. Existing collimation systems in high energy proton machines are, or were, all made of two-1D systems (see the caption of Figure III). No calculated or measured performance exist. The sole documented case is the HERA collimation system [4]. In all these studies, taking apart the 1D-case, the best arrangment of jaws was found for a predefined optic. The solutions found are therefore some kind of local mimina, in the hypothetical space of all possible optics.

In this paper we do not consider a particular optic. We rather derive the optical constraints between a primary jaw and its associated secondary ones which minimise the size of the secondary halo issued from the primary jaw. The constraints are expressed by correlated betatronic phase advances between primary and secondary jaws. The end result is an exact specification that an optic must satisfy to provide an optimum collimation system for a given number of jaws.

II. DEFINITION AND NOTATIONS

We use horizontal and vertical betatron coordinates as well as horizontal dispersion normalised with the transformations

$$\vec{X} = N_x\vec{x}, \;\; \vec{Y} = N_y\vec{y} \;\; \text{and} \;\; \vec{\chi} = N_x\vec{D}, \tag{1}$$

which expands as

$$\begin{pmatrix} X \\ X' \end{pmatrix} = \frac{1}{\sigma_x} \begin{pmatrix} 1 & 0 \\ \alpha_x & \beta_x \end{pmatrix} \begin{pmatrix} x \\ x' \end{pmatrix} \tag{2}$$

for X coordinates, and similarly for Y. We group $\vec{X}$ and $\vec{Y}$ in 4-vectors noted $\vec{A} = (X, X', Y, Y')$. The vector $\vec{A}$ is transported between two locations with $\vec{A}_2 = M_{12}\vec{A}_1$. The transfer matrix M_{12} is made of two clockwise rotations, one for each proper plane, where the angles of rotation μ_x and μ_y are the betatronic phase advances, i.e.

$$M_{12} = \begin{pmatrix} \cos\mu_x & \sin\mu_x & 0 & 0 \\ -\sin\mu_x & \cos\mu_x & 0 & 0 \\ 0 & 0 & \cos\mu_y & \sin\mu_y \\ 0 & 0 & -\sin\mu_y & \cos\mu_y \end{pmatrix}. \tag{3}$$

The normalised invariant amplitudes are

$$A_x = (X^2 + X'^2)^{1/2} \quad , \quad A_y = (Y^2 + Y'^2)^{1/2} \tag{4}$$

which can be added to form the combined betatronic invariant amplitude

$$A = (A_x^2 + A_y^2)^{1/2}. \tag{5}$$

III. BETATRON COLLIMATION

We first consider circular collimators in normalised coordinates. The normalised aperture of the primary and secondary collimators are n_1 and n_2 r.m.s transverse beam units respectively. These numbers are fixed in our problem, in the sense that n_1 cannot be varied to optimise a collimation system but must rather fit to external parameters like the dynamic aperture or the effective geometrical aperture of the ring. Similarly, we will see in Section III A that the relative retraction $(n_2 - n_1)/n_1$ must be kept constant once it has been chosen and shall therefore be substantially larger than for exemple local closed orbit changes. We use the approximation of slow transverse diffusion of the primary halo, with the consequence that the impact parameter at the primary collimator is small compared to n_1. More precisely said, we consider the impact points to be at the surface of the collimator while both betatronic oscillations are at their maxima, i.e. $X'_o = Y'_o = 0$ with $X_o^2 + Y_o^2 = n_1^2$. In Section III A we will minimise the extension of the secondary halo after it is cut by the secondary collimators treated as black absorbers, thus neglecting the formation of a tertiary halo.

With using the transverse azimuth α to define the point of impact on the primary collimator, the coordinates of the particles before scattering are

$$\vec{A}_o = (n_1 \cos\alpha, 0, n_1 \sin\alpha, 0). \tag{6}$$

The scattering process adds an arbitrary value to X'_o and Y'_o, using here for simplicity an isotropic distribution. With the use of the polar coordinates K and ϕ in the $X'_o - Y'_o$ plane (see Fig. 1), the coordinates at the primary collimator after scattering are

$$\vec{A}_1 = (n_1 \cos\alpha, K\cos\phi, n_1 \sin\alpha, K\sin\phi). \tag{7}$$

A. Phase advances

For arbitrary α and ϕ angles, we transport the particle with $\vec{A}_2 = M_{12}\vec{A}_1$ using Eqs. (3) and (7) to a location of yet unspecified phase advances μ_x and μ_y where a secondary collimator is located and get

$$\vec{A}_2 = \begin{pmatrix} n_1\cos\alpha\cos\mu_x + K\cos\phi\sin\mu_x \\ -n_1\cos\alpha\sin\mu_x + K\cos\phi\cos\mu_x \\ n_1\sin\alpha\cos\mu_y + K\sin\phi\sin\mu_y \\ -n_1\sin\alpha\sin\mu_y + K\sin\phi\cos\mu_y \end{pmatrix}. \tag{8}$$

The phases μ_x and μ_y are the free parameters of our problem. The efficiency of the secondary collimator is measured by the smallest amplitude $A_{2,cut}$ that it can intercept. $A_{2,cut}$ is minimised if X_2 and Y_2 are maximised, because the aperture of the secondary collimators is fixed to n_2. Using the invariance of $A_{x,2}$ and $A_{y,2}$, this condition is equivalent to asking for $X'_2 = Y'_2 = 0$. With these two conditions in Eq. (8) we get

$$\tan\mu_x = \frac{K\cos\phi}{n_1\cos\alpha} \quad , \quad \tan\mu_y = \frac{K\sin\phi}{n_1\sin\alpha}. \tag{9}$$

These conditions allow to compute the sole free parameters $\mu_x = \mu_x(\alpha,\phi,K)$ and $\mu_y = \mu_y(\alpha,\phi,K)$. While α and ϕ are free variables, K is restricted to its maximum allowed value corresponding to the smallest possible $A_{2,cut} = n_2$ (see Fig. 1). This is obtained by the substitution of Eqs. (9) in (8) with again $X'_2 = Y'_2 = 0$. We get

$$K = K_c = \sqrt{n_2^2 - n_1^2}, \tag{10}$$

which is independent of both α and ϕ. Writing

$$\tan\mu_o = K_c/n_1 = (n_2^2 - n_1^2)^{1/2}/n_1 \;\text{ or }\; \cos\mu_o = n_1/n_2 \;, \tag{11}$$

Eqs. (9) become

$$\tan\mu_x = \tan\mu_o\frac{\cos\phi}{\cos\alpha} \quad , \quad \tan\mu_y = \tan\mu_o\frac{\sin\phi}{\sin\alpha}. \tag{12}$$

The normalised angle K_c is the largest scattering angle which passes the secondary jaw and as it shall be, the corresponding largest amplitude is $A_{1,max} = A_{2,cut} = (n_1^2 + K_c^2)^{1/2} = n_2$. The two conditions stated by Eqs. (12) are our central result. They fix univoquely the location of a secondary jaw to cut the secondary amplitudes to its lower limit $A_2 = n_2$ for α and ϕ. They are governed by the single parameter μ_o (see also Table III). The phase μ_o depends on the choice of the ratio n_1/n_2. Therefore, this ratio must be fixed before chosing the optic of a cleaning insertion. Its value also fixes the location of all secondary collimators. These formulae indicate that an optimum collimation for all possible α and ϕ would need an infinity of collimators, with an optic able to offer an infinity of pairs of phase advances (μ_x, μ_y) which satisfy Eq. (12).

Before compromising on the number of collimators, it must be noticed that for given (α,ϕ), the secondary collimator at (μ_x, μ_y) needs not be circular. A single flat jaw at the $X - Y$ azimuth $\alpha_J = \tan^{-1}(X_2/Y_2)$ is sufficient (see Fig. 1). With Eq. (8), the azimuth of the jaw must be

$$\tan\alpha_J = \frac{\sin\alpha\cos\mu_y + \tan\mu_o\sin\phi\sin\mu_y}{\cos\alpha\cos\mu_x + \tan\mu_o\cos\phi\sin\mu_x}. \tag{13}$$

In practice, the transverse adjustment of the jaws, i.e. at either n_1 or n_2 beam units of the central orbit can only be made by the use of an opposite jaw in the same tank both together forming a pair with their respective azimuths α_J and $\alpha_J + \pi$ (see [5]). Therefore the determination of α_J by its tangent in Eq. (13) in the range $[-\pi/2, \pi/2]$ modulo π is univoque. For later use in Section III B we compute also

$$\cos\alpha_J = \frac{n_1}{n_2}\frac{\cos\alpha}{\cos\mu_x} \quad , \quad \sin\alpha_J = \frac{n_1}{n_2}\frac{\sin\alpha}{\cos\mu_y}. \tag{14}$$

The result is obtained for $\cos\alpha_J$ with $\cos\alpha_J = X_2/n_2 = (n_1/n_2)\cos\mu_x(\cos\alpha + K_c\tan\mu_x\cos\phi)$ and Eq. (14) then by rewriting Eq. (12) as $K_c/n_1 = \tan\mu_x\cos\alpha/\cos\phi$ and using $1 + \tan^2\mu_x = 1/\cos^2\mu_x$. The derivation is identical for $\sin\alpha_J = X_2/n_2$.

From now on we will consider flat collimators only.

B. Geometry of the secondary halo in the phase-space

For a given pair of primary impact and scattering angles (α, ϕ) and its associated secondary jaw located at optimised phase advances (μ_x, μ_y) oriented at the transverse azimuth α_J obtained respectively with Eqs. (12) and (13), we compute the domain of scattering angles at the primary collimator which are projected at the edge of the secondary jaw. The scattering angles in the $X'_1 - Y'_1$ plane are parametrised with the free azimuth ψ

$$K_x = K cos\psi \quad K_y = K sin\psi. \tag{15}$$

The edge of the secondary jaw is parametrised with

$$X_2 \cos \alpha_J + Y_2 \sin \alpha_J = n_2. \tag{16}$$

We rewrite X_2 and Y_2 from Eq. (8)

$$X_2 = n_1 \cos \alpha \cos \mu_x + K_x \sin \mu_x \tag{17}$$

$$Y_2 = n_1 \sin \alpha \cos \mu_y + K_y \sin \mu_y. \tag{18}$$

With Eqs. (17), (18) and (14) in (16) we get

$$K_x n_1 \cos \alpha \tan \mu_x + K_y n_1 \sin \alpha \tan \mu_y = n_2^2 - n_1^2 \tag{19}$$

Using Eqs. (10), (12) and the definition (11) we finally get

$$K_x \cos \phi + K_y \sin \phi = K_c \ , \tag{20}$$

which is the normalised equation of a line with K_c the shortest distance to the origin and ϕ its slope. With this result the effect of an optimised secondary jaw is easily interpreted. With K_c the smallest scattering angle cut when $\psi = \phi$ (remembering that the optimisation was done for the scattering angle ϕ), the line of Eq. (20) delimits a half plane of scattering angles $K_x \cos \phi + K_y \sin \phi > K_c$ intercepted by the jaw and the complementary half-plane $K_x \cos \phi + K_y \sin \phi < K_c$ passing the jaw. Several secondary jaws labelled with their central azimuth $(\alpha, \phi_i, i \, \epsilon \, [1, m_s])$ define a polygon of order m_s (if $m_s \geq 3$) which delimits the area of scattering angles which are not intercepted. The secondary halo is therefore delimited in the 4D-phase space at the location of the primary jaw by a 2D-polygon, labelled by the index m_s, located in a plane parallel to the axes X' and Y' at $(X_1 = n_1 \cos \alpha, Y_1 = n_1 \sin \alpha)$. This polygon has an inscribed circle of radius K_c. The largest amplitude of the secondary halo is therefore $A^2_{max}(m_s) = n_1^2 + K^2_{max}(m_s)$ with $K_{max}(m_s)$ the distance of the most remote apex of the polygon relative to the origin $X' = Y' = 0$ (see Fig. 2).

In addition to the optimisation made by using the correlated phase advances of Eq. (12), a second optimisation is now made by requesting that for given m_s the polygon be made regular. This minimises both $K_{max}(m_s)$ and the surface of the polygon. The scattering angles ϕ_i used to compute the phases of the secondary jaws shall therefore be equally distributed around the azimuth with $(\phi_i = \phi_o + i\pi/m_s, i \, \epsilon \, [1, m_s])$. Varying ϕ_o rotates the polygon but do not modify the distribution of the combined secondary amplitude. The angle ϕ_o can therefore be freely chosen as long as isotropic scattering is considered. But in practice the outscattering rate is largest at $\phi = \alpha + \pi$, a value to which one jaw must be adjusted by chosing ϕ_o adequately.

C. A finite number of collimators

In a real collimation system, both the number m_p of primary and m_s of secondary jaws must be finite and small. The choice of m_p and m_s is made a bit complicated by an effective correlation between them. We first discuss the case of the primary jaws.

1. Primary collimators

We considered circular collimators in Section III to simplify our calculations. In practice, it is also often desirable to define a circular primary aperture. One reason is to fit to a circular vacuum chamber which define an approximated circular normalised aperture when integrated over an arc cell. Another reason might be the need to fit to a nearly circular dynamic aperture. On the other hand in practice, the circular aperture must be approximated by flat jaws which have an adjustable distance to the beam. They shall be arranged to form a regular polygon, to limit at best the primary amplitudes above the specified value n_1 (see Fig. 3). The phase advances of the secondary jaws shall be computed for the central impact points of the primary jaws (see Fig. 3), defined by the central azimuths $(\alpha_i = (i-1)\pi/[2(m_p - 1)], \ i\epsilon[1, m_p])$. At the central location the primary aperture is $A_o = n_1$ while at the apex of the polygon it is

$$A_{o,max} = \frac{n_1}{cos[\frac{\pi}{4(m_p - 1)}]} \tag{21}$$

as deduced by trigonometry from Fig. 3. Primary impacts maps are of course not limited to the central point of the jaw but rather continuously distributed all along the surface of the jaws. For later use we define an approximate average primary amplitude over the whole azimuth α with

$$A_{o,eff}(m_p) = n_{eff}(m_p) = \frac{1}{2}\{(n_1 + \frac{n_1}{\cos[\frac{\pi}{4(m_p-1)}]})\}. \tag{22}$$

With only $m_p = 2$ primary jaws (usually oriented horizontally and vertically) the largest primary amplitude before scattering is $A_{o,max} = \sqrt{2}n_1 \simeq 1.41n_1$ (see Fig. 3), which is a too large value when high performance is mandatory. With $m_p = 3$ jaws, thus defining an octagonal primary aperture, a much better performance is obtained with $A_{o,max} = n_1/\cos(\pi/8) \simeq 1.08n_1$ (see Fig. 3).

2. Secondary collimators

To help chosing the number of secondary jaws we give for a set of m_s values in Table I the variable $K_{max}(m_s)$ discussed in Section III B, the associated maximum secondary amplitude $A_{2,max}(m_s)$ and the relative surface S/K_c^2 of the regular polygon which delimits the secondary halo in the phase-space. Numerical values are computed with $n_1 = 6$ and $n_2 = 7$. Any number m_s of secondary jaws can be considered but above $m_s = 4$ the changes per m_s unit are small. With $A_{2,max}(m_s = 3) = 9.4$ the case $m_s = 3$ can be readily be discarded and we further limit our discussion to $(m_p = 3, m_s = 4)$ and $(m_p = 3, m_s = 8)$. We must now take into account the effective primary amplitudes which limit the performance obtained by the secondary jaws. We therefore define an effective average of the maximum secondary amplitude

$$A_{eff,max}(m_p, m_s) = \sqrt{n_{eff}(m_p)^2 + \frac{1}{4}[K_c + K_{max}(m_s)]^2} \tag{23}$$

with $n_{eff}(m_p)$ taken from Eq. (22). We also define the total number of jaws

$$m_{jaws} = m_p(1 + m_s). \tag{24}$$

Both $A_{eff,max}$ and m_{jaws} are given in Table II.

The difference of the effective performance $\delta A_{max} = 0.3$ between the two cases $(m_p = 3, m_s = 4)$ and $(m_p = 3, m_s = 8)$ (see Table II) is marginal, ruling out the case $(m_p = 3, m_s = 8)$. To make full use of eight secondary jaws five primary ones must be considered, with a result close to the ultimate limit $A_{max} = n_2$, but at the price of a quite prohibitive number of jaws amouting to 45 (see Table II).

We therefore further consider the case $m_p = 3$ with $m_p = 4$ secondary collimators per primary one. The phases in Table III are computed with Eq. (12) for the central impacts on the primary jaws $\alpha = 0, \pi/4, \pi/2$ with four equidistant scattering angles $\phi_i = [\alpha + i\pi/2, i = 1, 4]$. Theses correlated phases constitute a specification for an optic to offer the smallest secondary halo extension for the given number of jaws.

D. Simulation for continuous primary impact

To check the relevance of the effective maximum amplitude of Eq. (23), we integrated numerically the amplitude distribution of the secondary halo with a simple simulation program. We used the primary and secondary apertures $n_1 = 6$ and $n_2 = 7$. Primary impacts are uniform along the inner surface of the jaws. Scattering angles are uniform in the $K - \phi$ plane. The tracking is made with the transfer matrix (3) in which the phases (μ_y, μ_x) are taken from Table III. At each collimator it is verified if the particle touches a jaw. The particles surviving all secondary collimators are added to a $A_x - A_y$ plot, thus building the density distribution $d^2N/dA_x dA_y$ of the secondary halo (see Fig. 4) and added also to a combined amplitude distribution dN/dA (see Fig. 5). The case $m_s = 8$ is also explored and added to Fig. 5. The effective maximum amplitude of Eq. (23) fits well to the end of the distribution dN/dA and is therefore a good indicator of the limit of the secondary halo. The distributions shown in Fig. 5 confirm that the case $(m_s = 3, m_p = 8)$ is not worth the additional hardware investment while four secondary collimators for each of the primary azimuths, i.e. twelve ones with three primary collimators is a quite good choice. This result was already obtained by D. Kaltchev who developped a numerical algorithm to minimise the size of a polygon in the $X' - Y'$ plane [3] [6].

E. Existing solutions

With a symmetric optic $(\mu_x(s) = \mu_y(s))$ the secondary halo is cut at $A_{sec} = 1.32n_2$ [2] with a ratio $n_2/n_1 = 7/6$. The present best performance obtained with a modulated optic for the LHC collimation insertion is $A_{sec} = 1.21n_2$

[3]. It was emphasized in former studies [2] [3] that cutting efficiently on large amplitudes associated to orthogonal scattering ($\phi = \alpha \pm \pi/2$) requires large phase modulation, i.e. large $\mu_y - \mu_x$ values, along the cleaning insertion. This argument was right but incomplete. Strict correlation of the phase advances μ_x and μ_y is mandatory and the maximum modulation $\mu_y - \mu_x = \pi/2$ is needed for some jaws (see Table III). While it may be unfair to compare the performance of existing optics to our nearly ultimate limit $A_{max,eff} = 1.08 n_2$ obtained with a yet virtual optic, a potential gain remains to be exploited with an optic which satisfies the phase advances specified in Table III.

F. Isotropic and real scattering

If the use of isotropic scattering is adequate for comparing different jaw arrangements, real scattering must be considered to quantify the performance of a system in absolute terms. We give here only a brief outlook of a discussion made in [1]. In first approximation elastic scattering of protons in matter is dominated by multiple Coulomb scattering. The angular distribution after scattering of a proton of momentum p through one interaction length of matter is Gaussian with a r.m.s width $\sigma'_{mcs} = ap^{-1} \simeq 3 \times 10^{-5} p^{-1}$ [rad,TeV/c] considering here an aluminum jaw. The quantity σ'_{mcs} is compared to the r.m.s beam divergence $\sigma'_\beta = (\epsilon_n m_p/\beta p)^{1/2} = bp^{-1/2} \simeq 6 \times 10^{-6} p^{-1/2}$ rad with the proton mass $m_p = 0.94 \times 10^{-3}$ Tev/c^2 and an average betatronic wave length $\beta \simeq 100$ m. In a proton collider we use a normalised emmitence $\epsilon_n \simeq 4 \times 10^{-6}$ m. The isotropic scattering model is adequate if the real scattering distribution is wider than the angular cut K_c made by the collimators, i.e. if

$$\sigma'_{mcs} \ \geq \ K_c \sigma'_\beta, \tag{25}$$

with K_c taken from Eq. (11). With $n_1 = 6$ and $n_2 = 7$ the cross-over momentum $p = (a/K_c b)^2 \simeq 2$ TeV/c deduced from the equality in Eq. (25) defines the limit below which the condition (25) is satisfied. Above this momentum, the isotropic model substantially overestimates the size of the secondary halo cut by the collimators. At the injection momentum of LHC, or $p = 0.45$ TeV/c, the performance of the cleaning insertion is $A_{isotropic,cut} = 8.4$ [3]. The limit obtained with a numerical model which includes real scattering, tertiary halo and multiturn tracking is $A_{cut} = 8.0$ [1], a slightly better value than the result obtained with the isotropic model. This indicate that the range of the cross-over momentum is quite large.

G. Secondary halo and quench levels

The link between the edge of the secondary halo and the quench levels in superconducting magnets is not direct. It is discussed in [1] and briefly outlined here. An aperture limitation in the ring delimits a small volume in phase-space, in which protons will be captured locally. The integral of the flux of halo in that small volume must be compared to the quench limit. If the edge A_{cut} of the distribution dN/dA of the secondary halo is smaller than the aperture of the ring A_{ring}, the secondary halo induces no direct losses. Tertiary losses, made of protons elastically scattered off the secondary collimators must then be considered and compared to the quench limit. On the other hand, it is always important to satisfy the condition $A_{cut} < A_{ring}$, because of the steep slope of dN/dA (see Fig. 5).

IV. MOMENTUM COLLIMATION

We restrict our discussion to a momentum cleaning insertion installed in a straight section, where the dispersion function is a betatronic trajectory. In that case, the condition $D'/D = -\alpha_x/\beta_x$, or equivalently $\chi' = 0$ (see Eqs. (1) and (2)), must be satisfied at the primary collimator [2] [7] to ensure that the cut made on the secondary halo does not depend on the relative momentum offset δ_p. It also strictly reduces the treatment of the momentum collimation to the betatronic case in a straight section [2], while outside the straight section the transverse offset x_β and $x_{\delta_p} = D\delta_p$ must of course be distinguished.

In the usual case of a ring without substantial vertical dispersion and in contrast with the betatron halo which may drift away from the beam in all transverse directions, momentum losses are concentrated in the horizontal plane. The most demanding case occurs at ramping when off-bucket protons are lost. Most of these protons keep their initial betatronic amplitude at injection [8] and are therefore confined in the range of betatronic amplitudes $A_{x,y} \approx 2$. It is therefore enough to use a single horizontal primary collimator, to which four secondary collimators must be associated, following the conclusions of Section III C. Their locations correspond to the case $\alpha = 0$ of Table III and they limit the components of the betatron vector after scattering to $\vec{A}_1 = (n_1, K_c, \approx 2, K_c)$.

In the arc of a ring, the aperture limitation for a particle with momentum offset is located near horizontally focusing quadrupoles where both β_x and D_x are at their maximum. With in addition $\beta_y \ll \beta_x$, it is thus adequate to fit the largest horizontal secondary excursions $A_{x,\beta} + D\delta_p$ of the secondary halo with the aperture $N_{arc} = N_{x,arc}$ at that location. The straight sections of a ring need not be considered for momentum collimation since the dispersion is usually supressed in these areas.

A. Amplitude cut with momentum offset

In the general case, a particle reaches the primary collimator with a mixing of betatron amplitude and momentum offset. With the dispersion χ_1 at the primary collimator, and using the approximation of slow diffusion (see section III) we write

$$n_1 = \chi_1\delta_p + X_\beta = \chi_1\delta_p + A_{x,\beta} \tag{26}$$

and define the largest momentum offset which can pass the primary collimator as $\delta_c = n_1/\chi_1$ with $A_{x,\beta} = 0$. After scattering and the cut of the amplitude by the secondary collimators, the maximum horizontal betatronic amplitude is $A_{x,\beta} = [(n_1 - \chi_1\delta_p)^2 + K_c^2]^{1/2}$. Expanding $A_{x,\beta}$ with Eq. (10), the maximum horizontal excursion in the arc is

$$X_{max}(n_1, \chi_1, \delta_p) = \chi_{arc}\delta_p + (\chi_1^2\delta_p^2 - 2n_1\chi_1\delta_p + n_2^2)^{1/2} \tag{27}$$

and is plotted in Fig. 6. The largest allowed excursion $X_{max}(n_1, \chi_1, \delta_c) = N_{arc}$ fixes

$$\delta_c(n_1) = n_1/\chi_1 = [N_{arc} - (n_2^2 - n_1^2)^{1/2}]/\chi_{arc} \tag{28}$$

obtained with $\delta_p = \delta_c(n_1)$ in Eq. (27). Would large n_1 values be considered (see Fig. 6), the large X_{max} excursion at small δ values would be cut at the betatron cleaning insertion. The system is completely fixed by chosing n_1 and computing the dispersion which is needed at the primary collimator

$$\chi_1(n_1) = \frac{n_1}{\delta_c} = \frac{n_1\chi_{arc}}{N_{arc} - (n_2^2 - n_1^2)^{1/2}}. \tag{29}$$

As for the choice of n_1, a lower limit $n_{1,min}$ is fixed by the acceptable effective cut of the primary horizontal betatronic amplitude at the edge of the bucket $n_{edge} = n_1(1 - \delta_b/\delta_c)$ with δ_b the bucket width. In practice, a high enough χ_1 must be obtained by matching the optic such that the corresponding n_1 value obtained with Eq. (29) is larger than $n_{1,min}$.

V. SUMMARY

We derived the correlated betatronic phase advances between primary and secondary jaws which allow to cut the amplitude of the secondary halo of a two-stage collimation system down to the aperture of the secondary collimators. We showed that an infinite number of jaws would be necessary to reach that limit. We derived a precise estimator of the effective extension of the secondary halo for a finite number of jaws. We give a specification that an optic must satisfy for the case of a collimation system made of three primary jaws and twelve secondary ones. We also specified the properties of a momentum cleaning insertion.

ACKNOWLEDGEMENTS

The author is indebted to T. Trenkler who pointed him to Eq. (20) and to part of the subsequent deductions and to D. Kaltchev with whom I had numerous useful discussions.

[1] N. Catalan Lasheras et al., *Proceedings of the Symp. 'Near Beam Physics', Fermilab, 1997*, edited by D. Carrigan and N. Mokhov, p. 117 and CERN LHC Project Report 156, 1998.
[2] T. Trenkler and J. B. Jeanneret, Part. Acc. **50**, 287 (1995).
[3] D. I. Kaltchev et al., *Proceedings of the PAC97 Conference, Vancouver, 1997*, edited by M. K. Craddock et al., p. 1432 and CERN LHC Project Report 37, 1996., p. 153 and CERN LHC Project Report 134, 1997.
[4] M. Seidel, Desy 94-103, Hamburg, 1994.
[5] N. Catalan Lasheras, G. Ferioli and J. B. Jeanneret, *Proceedings of the EPAC98 Conference, Stockholm, 1998*, edited by S. Myers et al., p. 242 and CERN LHC Project Report 185, 1998.
[6] D. I. Kaltchev et al., *Proceedings of the EPAC96 Conference, Sitges, 1996*, edited by S. Myers et al., p. 1432 and CERN LHC Project Report 37, 1996.
[7] P. J. Bryant and E. Klein, CERN SL report 92-40, 1992.
[8] N. Catalan Lasheras, CERN LHC Project Report 200, 1998.

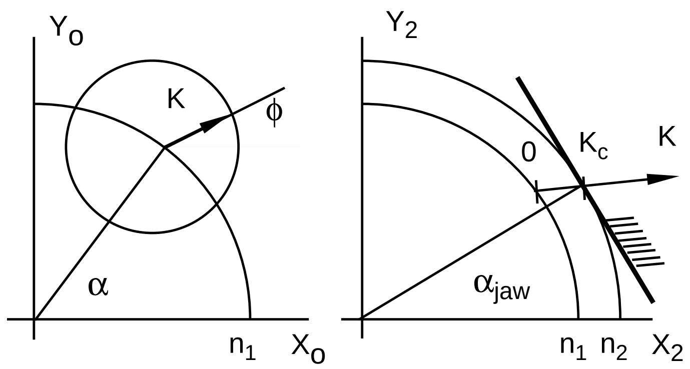

FIG. 1. The line of the scattered particles at the primary collimator parametrised with (n_1, α, K, ϕ) transforms at the location of a secondary collimator to another line which crosses the circle of radius n_2 when $K = K_c$ whatever α and ϕ, see Eq. (11). A flat jaw at azimuth α_{jaw} is sufficient to cut at amplitude $A = n_2$, see text.

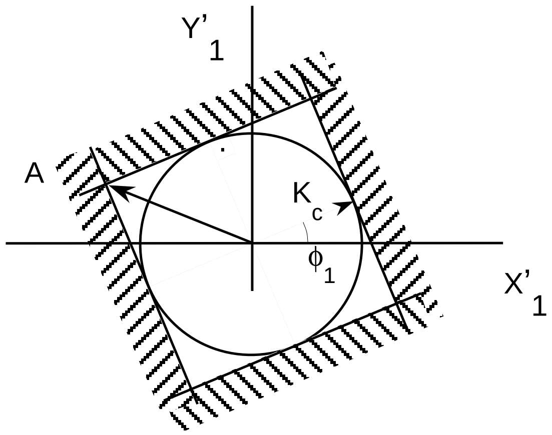

FIG. 2. The polygon delimited by the secondary jaws in the $X' - Y'$ plane. Here $m_s = 4$. The scattering azimuth are chosen equidistant to form a square which minimises the surface and the extention of the polygon. The largest angle passing the secondary jaws is $K_{4,max} = \|OA\| = \sqrt{2}K_c$.

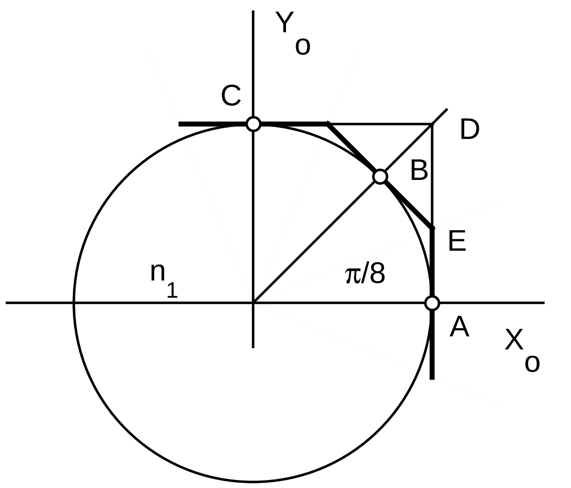

FIG. 3. The $X - Y$ primary impact distribution of the simulation on the primary collimator jaws. The small circles are the scattering sources of the central impact approximation for which the betatronic phase advances were computed (see text). With $m_p = 2$, the largest amplitude before scattering is already $A_{o,max} = \|OD\| = \sqrt{2}n_1$. With $m_p = 3$, the jaws being arranged to form an octagonal primary aperture, $A_{o,max} = \|OE\| = n_1/cos(\pi/8) = 2n_1/(2 + \sqrt{2})^{1/2}$.

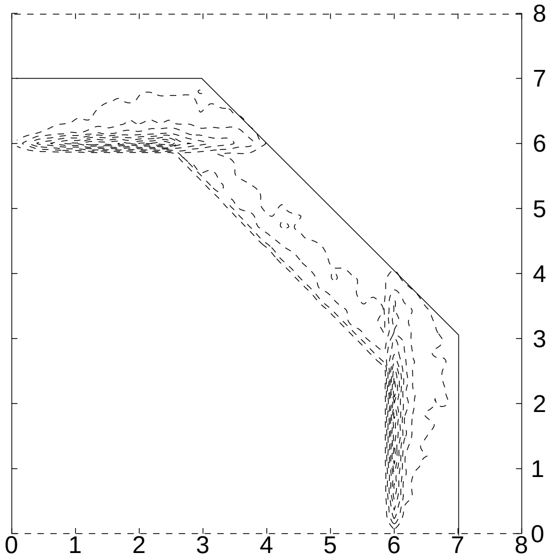

FIG. 4. The contour plot of the distribution d^2N/dA_xdA_y of the secondary halo in the case $m_p = 3$ and $m_s = 4$ with continuous primary impact distribution. This distribution is obtained with isotropic scattering. The abscissa is A_x and the ordinate A_y. We used collimator apertures $n_1 = 6$ and $n_2 = 7$. The two octagons of inner radii n_1 and n_2 indicate that the secondary halo is almost entirely contained inside these limits.

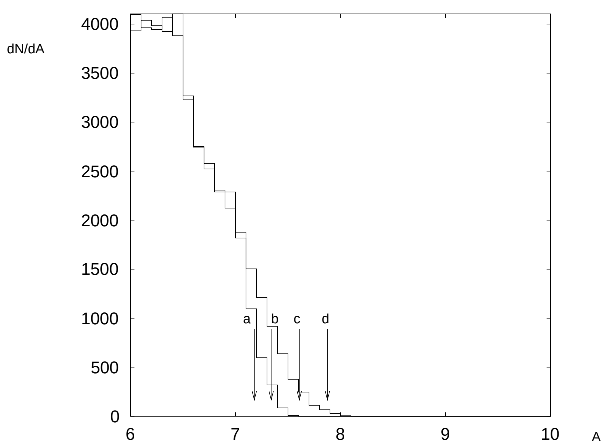

FIG. 5. The distribution dN/dA for $m_p = 3$ and $m_s = 4$ (upper curve) compared to $m_p = 3$ and $m_s = 8$ (lower curve). We used collimator apertures $n_1 = 6$ and $n_2 = 7$. In abscissa, the combined amplitude in normalised units. This distribution is obtained with isotropic scattering. The arrows a and d correspond to $A_{4,max}$ and $A_{8,max}$ computed with central impacts and are taken from Table II. The arrows b and c are the effective limits of Eq. (23) for the same two cases. The latter ones are much better estimators of the upper limits if the fading ends of the spectra are neglected.

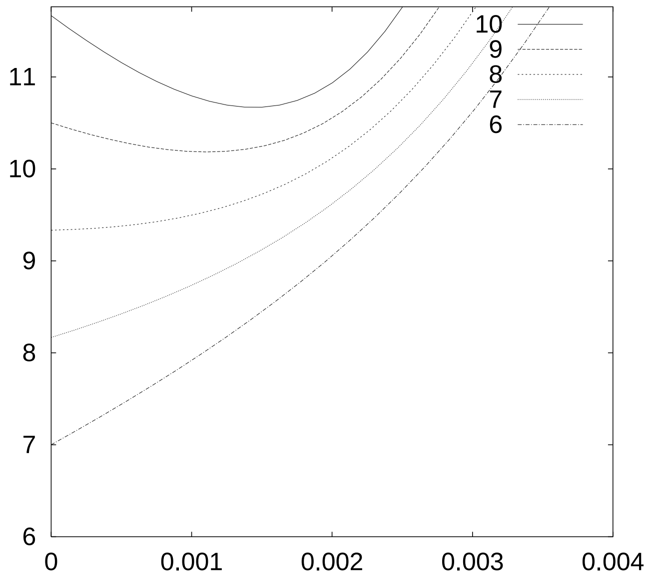

FIG. 6. The maximum transverse normalised excursion X_{max} (ordinate) of a particle as a function of the relative momentum offset δ_p (abscissa) and of the primary collimator aperture n_1 (index in the right upper corner of the figure). Each curve is ended at $\delta_p = \delta_c(n_1)$ where $X_{max} = N_{arc} = 11.8$, a case study for LHC for which we fixed the ratio $n_2/n_1 = 7/6$.

TABLE I. Extension of the secondary halo for different numbers m_s of pairs of secondary jaws per primary impact point. The variable m_s is also the order of the polygon discussed in Section III B. The expressions for K_{max} are obtained by the geometry of regular polygons and the maximum amplitudes are given by $A_{max}^2 = n_1^2 + K_{max}^2$. We used the collimator apertures $n_1 = 6$ and $n_2 = 7$ to compute A_{max} numerically.

m_s	K_{max}	A_{max}^2	A_{max}	S/K_c^2	S/K_c^2
3	$2K_c$	$4n_2^2 - 3n_1^2$	9.4	$3\sqrt{3}$	5.19
4	$\sqrt{2}K_c$	$2n_2^2 - n_1^2$	7.9	4	4.00
8	$2K_c/(2+\sqrt{2})^{1/2}$	$(4n_2^2 - 2n_1^2 + \sqrt{2}n_1^2)/(2+\sqrt{2})$	7.2	$8\sqrt{\frac{2-\sqrt{2})}{2+\sqrt{2})}}$	3.31
∞	K_c	n_2	7	π	3.14

TABLE II. Effective maximum amplitude of the secondary halo $A_{max,eff}$ and total number of jaws m_{jaws} as a function of the number of primary and secondary jaws m_p and m_s. The primary jaws are arranged to form a regular polygon in the normalised plane (X_1, Y_1). The secondary jaws are arranged to contain the scattering angles inside another regular polygon located in the normalised plane (X_1', Y_1'). The betatronic phase advances between primary and secondary jaws are the optimum ones, see text.

m_p	m_s	$A_{max,eff}$	m_{jaws}
3	4	7.6	15
3	8	7.3	27
5	4	7.5	25
5	8	7.1	45

TABLE III. Secondary collimator locations μ_x and μ_y and jaw orientations α_J for three scattering azimuths α and four scattering angles ϕ . One can add π to any of these phases but then α_{jaw} must be reevaluated. It is assumed that jaws are mounted in transversely opposite pairs, i.e. for each entry in the table there is a jaw at α_J and one at $\alpha_J + \pi$, for operational reasons explained in Section III A. We listed the value α_J which is closer to the first quadrant. The lines of the table where $\phi = \alpha$ or $\phi = \alpha + \pi$ correspond to plane scattering and define a 1D-collimation system. The existing collimation systems in proton colliders cut on plane scattering and only with horizontal and vertical primary jaws, i.e. have primary and secondary jaws corresponding to lines 1,2,9 and 10 of the table.

α	ϕ	μ_x	μ_y	α_J
0	0	μ_o	-	0
0	π	$\pi - \mu_o$	-	0
0	$\pi/2$	π	$3\pi/2$	μ_o
0	$-\pi/2$	π	$3\pi/2$	-μ_o
$\pi/4$	$\pi/4$	μ_o	μ_o	$\pi/4$
$\pi/4$	$5\pi/4$	$\pi - \mu_o$	$\pi - \mu_o$	$\pi/4$
$\pi/4$	$3\pi/4$	$\pi - \mu_o$	$\pi + \mu_o$	$\pi/4$
$\pi/4$	$-\pi/4$	$\pi + \mu_o$	$\pi - \mu_o$	$\pi/4$
$\pi/2$	$\pi/2$	-	μ_o	$\pi/2$
$\pi/2$	$-\pi/2$	-	$\pi - \mu_o$	$\pi/2$
$\pi/2$	π	$\pi/2$	π	$\pi/2 - \mu_o$
$\pi/2$	0	$\pi/2$	π	$\pi/2 + \mu_o$